J|A|C|S
COMMUNICATIONS

Published on Web 02/07/2007

# Electrochemical Oxidation of Water by an Adsorbed $\mu$-Oxo-Bridged Ru Complex

Feng Liu,[†] Thomas Cardolaccia,[†] Brooks J. Hornstein,[§] Jon R. Schoonover,[§] and Thomas J. Meyer*[,†]

*Department of Chemistry, CB #3290, University of North Carolina, Chapel Hill, North Carolina 27599, and Materials Science and Technology, MS E549, Los Alamos National Laboratory, Los Alamos, New Mexico 87545*

Received December 1, 2006; E-mail: tjmeyer@unc.edu

Light-driven catalytic water oxidation occurs as the terminal step in photosystem II at the oxygen evolving complex (OEC) and is a potential half-reaction for artificial photosynthesis and photochemical energy conversion based on water splitting.[1] Molecular catalysts for water oxidation have been described including polypyridyl complexes of ruthenium, such as the extensively studied blue $\mu$-oxo Ru dimer, *cis,cis*-$[(bpy)_2(H_2O)Ru^{III}ORu^{III}(OH_2)(bpy)_2]^{4+}$ (bpy is 2,2′-bipyridine),[2] and more recently, related complexes of Ru based on bridging pyridyl-type ligands.[3] An example of stoichiometric water oxidation by the $\mu$-oxo-bridged terpyridyl complex, $[(tpy)(H_2O)_2Ru^{III}]_2O^{4+}$ (**1**) (tpy = 2,2′:6′,2″-terpyridine), has also been reported.[4] In these complexes, oxidation and proton loss by proton-coupled electron transfer (PCET) occurs from the lower oxidation state aqua and hydroxo precursors to give reactive high oxidation state Ru=O species such as $[(bpy)_2(O)Ru^{V}]_2O^{4+}$, which are the active forms for water oxidation.[5]

Here we describe extension of the $\mu$-oxo-based water oxidation chemistry to metal oxide surfaces based on the phosphonate-modified complex, $[(tpy\text{-}PO_3H_2)(H_2O)_2Ru^{III}]_2O^{4+}$ (**2**) (tpy-$PO_3H_2$ is 4′-phosphonato-2,2′:6′,2″-terpyridine). Our results demonstrate that **2** retains its PCET and water oxidation properties on oxide surfaces, including $TiO_2$ which has been used extensively in dye-sensitized solar cells.[6]

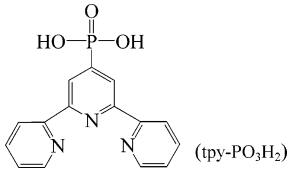

(tpy-$PO_3H_2$)

The ligand tpy-$PO_3Et$ and complex Ru(tpy-$PO_3Et_2$)($C_2O_4$)($H_2O$) ($C_2O_4^{2-}$ is the oxalato ligand) were synthesized by literature procedures and purified by chromatography on Sephadex LH-20.[4,7] Stirring this complex in water at 80 °C for 2 h in the presence of 10 equiv of $NaClO_4$ as the oxidizing agent afforded the $\mu$-oxo complex $[(tpy\text{-}PO_3Et_2)(C_2O_4)Ru^{III}]_2O$, which was purified on Sephadex LH-20. The $^1$H NMR of $[(tpy\text{-}PO_3Et_2)(C_2O_4)Ru^{III}]_2O$ was consistent with the reported NMR data of **1**, and in $^{31}$P NMR, only one peak was displayed at 6.12 ppm (vs external $KPF_6$ aqueous solution, Supporting Information Figure S1). As for **1**, the geometry at the metal in this complex is presumably *mer* with regard to the Ru−O−Ru axis. Finally, hydrolysis of the oxalato ligand and the phosphonate esters was achieved by refluxing the complex in 2 M triflic acid under Ar for 2 days to obtain **2**. This solution was then diluted and used as a stock solution for surface binding.

Stable phosphonate surface binding of **2** on ITO (Sn(IV)-doped $In_2O_3$) and on films (~10 $\mu$m thickness) of nanoparticle (10−20 nm) $ZrO_2$, $TiO_2$, or $SnO_2$ on ITO occurred following exposure of oxide electrodes to a $\sim 2.5 \times 10^{-4}$ M stock solution in **2** in aqueous triflic acid solution at pH ~ 1. Saturation coverage of $7 \times 10^{-11}$ mol/cm$^2$ on ITO was achieved in about 4 h as monitored by the area under the cyclic voltammetric wave for the $Ru^{IV}-O-Ru^{III}$/$Ru^{III}-O-Ru^{III}$ couple at $E_{1/2}$ = 0.52 V vs Ag/AgCl in pH = 1 triflic acid.[8] The extent of surface loading on metal oxide nanoparticles was estimated by UV−visible measurements by using the aqueous solution value of $\epsilon = 8 \times 10^3$ M$^{-1}$ cm$^{-1}$ at $\lambda_{max}$ = 694 nm for **2**. Typical surface coverages after ~16 h exposure times were $1.2 \times 10^{-7}$ mol/cm$^2$ for ITO|$ZrO_2$ and ITO|$TiO_2$ and $5 \times 10^{-8}$ mol/cm$^2$ for ITO|$SnO_2$.

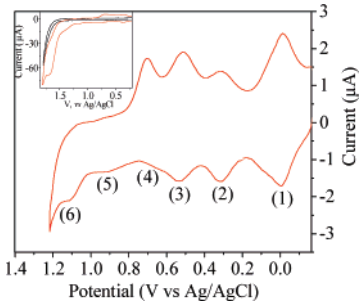


***Figure 1.*** Cyclic voltammograms of complex **2** (red lines) on ITO, in pH 5.0 buffer solution ($I$ = 0.1 M, $CH_3CO_2H/CH_3CO_2Na$) at a scan rate of 40 mV/s vs Ag/AgCl (0.197 V vs NHE). Also shown in the inset is the CV of the ITO background (black line) at the same scan rate. See text for assignment of the waves.

Cyclic voltammograms (CV) of **2** on ITO electrodes, ITO|**2**, are dependent on pH, scan rate, and the composition and concentration of the external buffer solution. CVs of ITO|**2** and ITO|$ZrO_2$|**2** in pH 5.0 buffer solution ($I$ = 0.1 M, $CH_3CO_2H/CH_3CO_2Na$) are shown in Figure 1 and Supporting Information Figure S2. Comparison with solution results on **1** indicates the following assignments for the numbered waves in Figure 1 in volts versus Ag/AgCl:[4] (1) 2e$^-$ $Ru^{III}-O-Ru^{III}/Ru^{II}-O-Ru^{II}$ couple at −0.01 V; (2) $Ru^{IV}-O-Ru^{III}/Ru^{III}-O-Ru^{III}$ at 0.32 V; (3) $Ru^{IV}-O-Ru^{IV}/Ru^{IV}-O-Ru^{III}$ at 0.52 V; (4) $Ru^{V}-O-Ru^{IV}/Ru^{IV}-O-Ru^{IV}$ at 0 .68 V; (5) $Ru^{V}-O-Ru^{V}/Ru^{V}-O-Ru^{IV}$ at 0.93 V; and (6) $Ru^{VI}-O-Ru^{V}/Ru^{V}-O-Ru^{V}$ at 1.09 V. The $Ru^{VI}-O-Ru^{V}/Ru^{V}-O-Ru^{V}$ wave was not observed in earlier solution measurements on **1**.[4]

On the basis of the pH dependence of $E_{1/2}$ values in Supporting Information Figure S3 and earlier solution results,[4] the proton composition of $Ru^{V}-O-Ru^{V}$ could be either ITO|$[(tpy\text{-}PO_3H_2)(H_2O)(O)Ru^{V}]_2O^{4+}$ or ITO|$[(tpy\text{-}PO_3H_2)(HO)_2Ru^{V}]_2O^{4+}$ at pH = 5. As in previous studies, the implied slow kinetics for the higher oxidation state couples is a consequence of PCET, perhaps due to slow proton loss in the formation of $Ru^{V}$=O.[5]

As illustrated in Figure 1, there is evidence for catalytic currents at potentials past the waves for oxidation of $Ru^{V}-O-Ru^{IV}$ to

[†] University of North Carolina.
[§] Los Alamos National Laboratory.


10.1021/ja068630+ CCC: $37.00 

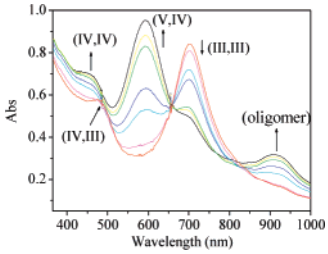


***Figure 2.*** Changes in absorption spectrum of **2** on $TiO_2$ with time and applied potential of 1.05 V vs Ag/AgCl in pH 1 $HPF_6$ under Ar.

$Ru^{V}-O-Ru^{V}$ (5) and of $Ru^{V}-O-Ru^{V}$ to $Ru^{VI}-O-Ru^{V}$ (6). There is evidence for an additional oxidative wave, presumably for the $Ru^{VI}-O-Ru^{VI}/Ru^{VI}-O-Ru^{V}$ couple on the current plateau at ~1.65 V (inset Figure 1). Catalytic currents were also observed in nanoparticle films of **2** as ITO|$TiO_2$|**2**, ITO|$ZrO_2$|**2**, and ITO|$SnO_2$|**2**.

As observed for related solution couples, $E_{1/2}$ values vary with pH (Supporting Information Figure S3). For example, $E_{1/2}$ for the $Ru^{IV}-O-Ru^{III}/Ru^{III}-O-Ru^{III}$ couple decreases by ~50−60 mV/pH unit from pH 0 to 6.2, consistent with the PCET half-reaction in eq 1.

$$\mathrm{ITO|[(tpy\text{-}PO_3H_2)(H_2O)(HO)Ru^{IV}ORu^{III}(OH_2)_2(tpy\text{-}PO_3H_2)]^{4+} + e^- + H^+ \rightarrow ITO|[(O_3H_2P\text{-}tpy)(H_2O)_2Ru^{III}]_2O^{4+}} \quad (1)$$

As for the solution analogue, reduction of $Ru^{III}-O-Ru^{III}$ to $Ru^{II}-O-Ru^{II}$ at $E_{app} = -0.1$ V at pH = 1 results in reductive cleavage to give ITO|2{$[(tpy\text{-}PO_3H_2)Ru^{II}(H_2O)_3]^{2+}$}, with some loss of monomer. This is shown in the resulting CV by the appearance of characteristic monomer waves at 0.55, 0.80, and 1.02 V and by the appearance of a MLCT absorption at 560 nm.[9] The dimer reforms upon electrolysis at 0.9 V, past $E_{1/2}$ for the Ru(IV/III) wave, to give ITO|$[(tpy\text{-}PO_3H_2)(H_2O)_2Ru^{IV}ORu^{IV}(OH)(OH_2)(tpy\text{-}PO_3H_2)]^{5+}$. This demonstrates that the near-neighbor structure on the surface is retained after cleavage of the $\mu$-oxo bridge.

The progression of the surface complex from $Ru^{III}-O-Ru^{III}$ to higher oxidation states was monitored spectroelectrochemically. Holding the electrode potential at 0.65 V resulted in a decrease in $Ru^{III}-O-Ru^{III}$ absorption at $\lambda_{max} = 702$ nm with a corresponding increase for $Ru^{IV}-O-Ru^{III}$ at 485 nm (Figure S4), in good agreement with the corresponding $Ru^{IV}-O-Ru^{III}$ form of **1** in solution.[4] At 1.05 V, new absorption bands appeared at 475, 592, and 910 nm (Figure 2). The former are attributable to $Ru^{IV}-O-Ru^{IV}$ and $Ru^{V}-O-Ru^{IV}$. The latter may be due to an oligomer given the related chemistry that appears in concentrated solutions of oxidized **1** arising from $Ru^{IV}-O-Ru^{IV}$ coupling.[4] This absorption feature is greatly decreased as surface coverage is decreased.

Electrocatalytic water oxidation by $Ru^{V}-O-Ru^{V}$ and $Ru^{VI}-O-Ru^{V}$ was investigated on high surface area ~10 $\mu$m thick $ZrO_2$ films on FTO (fluorine-doped tin oxide), FTO|$ZrO_2$|**2**. In these experiments, the electrode potential was held past the $Ru^{V}-O-Ru^{V}/Ru^{V}-O-Ru^{IV}$ and $Ru^{VI}-O-Ru^{V}/Ru^{V}-O-Ru^{V}$ waves at both pH = 1.0 (triflic acid) and 6.0 (terephthalic acid/monoterephthalate anion buffer) under Ar. Both current−time profiles and evolved $O_2$ were monitored, the latter by using an AD Instruments micro-oxygen electrode interfaced to a Keithley 6517A electrometer situated in the Ar headspace in a locally designed airtight cell. Water oxidation was initiated by stepping the applied potential to 1.5 or 1.25 V at pH = 1, and at 1.32 or 1.15 V at pH = 6. The initial relatively high catalytic currents fell to ~10% of their initial values within 30 min and 1 h for $Ru^{V}-O-Ru^{V}$ and $Ru^{VI}-O-Ru^{V}$, respectively. The total volume of $O_2$ was calculated on the basis of the volume of the headspace and a calibration curve for the electrode and was corrected by including dissolved $O_2$ by using a method provided by the electrode manufacturer. Turnover numbers were calculated based on surface coverages $\Gamma = A/(10^3 \times \epsilon_{max})$ (mol/cm$^2$), where $A$ is the absorbance at the absorption maximum for $Ru^{III}-O-Ru^{III}$ and the surface area is in square centimeters.

Turnover numbers based on evolved oxygen were 1.8 (pH = 1) and 3.0 (pH = 6) for $Ru^{VI}-O-Ru^{V}$ and ~1 (pH = 1) and 2.6 (pH = 6) for $Ru^{V}-O-Ru^{V}$. Spectral scans, taken after completion of the water oxidation reaction, provide insight into the catalyst deactivation mechanism. After electrolysis at pH = 1, the surface contained (1) a modified form of $Ru^{IV}-O-Ru^{IV}$ and $Ru^{IV}-O-Ru^{IV''}$, with $\lambda_{max} = 470$ nm compared to $\lambda_{max} = 475$ nm for $Ru^{IV}-O-Ru^{IV}$, which may be anated with coordinated triflate ($CF_3SO_3^-$) as suggested for **1** in solution; (2) the putative oligomer at $\lambda_{max} = 910$ nm; (3) a modified, possibly anated form of $Ru^{V}-O-Ru^{IV}$ with $\lambda_{max} = 593$ nm; and (4) as shown electrochemically, the Ru(VI) monomer FTO|$ZrO_2$|$[(tpyPO_3H_2)Ru^{VI}(O)_2(H_2O)]^{2+}$ formed by oxidative cleavage of $Ru^{VI}-O-Ru^{V}$. Oxidative cleavage also occurs with Ce(IV) oxidation of **2** on $ZrO_2$ and for **1** in solution.[4] After a period of ~24 h, the surface stabilizes with a modified form of $Ru^{III}-O-Ru^{III}$ with $\lambda_{max} = 718$ nm dominant on the surface with evidence for possible oligomers having $\lambda_{max} =$ 820 and 910 nm (Figure S5).

Our results are significant in demonstrating that single electron transfer activation of multiple electron transfer and water oxidation can be transferred to the electrode interface on oxide electrodes. Although the extent of catalytic activity is limited, the origins of catalyst deactivation are reasonably well understood and point to the evolution of a related, robust family of surface-bound catalysts for water oxidation.

**Acknowledgment.** Funding support for this research by the University of North Carolina and Chemical Sciences, Geosciences and Biosciences Division, Office of Basic Energy Sciences, U.S. Department of Energy is gratefully acknowledged.

**Supporting Information Available:** CV of **2** on $ZrO_2$, $E_{1/2}$ of **2** on ITO versus pH, and additional spectroelectrochemical data. This material is available free of charge via the Internet at http://pubs.acs.org.

## References

(1) (a) Alstrum-Acevedo, J. H.; Brennaman, M. K.; Meyer, T. J. *Inorg. Chem.* **2005**, *44*, 6802. (b) Tommos, C.; Babcock, G. T. *Acc. Chem. Res.* **1998**, *31*, 18. (c) Meyer, T. J.; Huynh, M. H. V.; Thorp, H. H. *Angew. Chem., Int. Ed.* Accepted for publication. (d) McEvoy, J. P.; Brudvig, G. W. *Chem. Rev.* **2006**, *106*, 4455.
(2) (a) Gilbert, J. A.; Eggleston, D. S.; Murphy, W. R., Jr.; Geselowitz, D. A.; Gersten, S. W.; Hodgson, D. J.; Meyer, T. J. *J. Am. Chem. Soc.* **1985**, *107*, 3855. (b) Yamada, H.; Siems, W. F.; Koike, T.; Hurst, J. K. *J. Am. Chem. Soc.* **2004**, *126*, 9786. (c) Yang, X.; Baik, M. H. *J. Am. Chem. Soc.* **2006**, *128*, 7476. (d) Binstead, R. B.; Chronister, C. W.; Ni, J.; Hartshorn, C. M.; Meyer, T. J. *J. Am. Chem. Soc.* **2000**, *122*, 8464.
(3) (a) Zong, R.; Thummel, R. P. *J. Am. Chem. Soc.* **2005**, *127*, 12802. (b) Masllorens, E.; Rodriguez, M.; Romero, I.; Roglans, A.; Parella, T.; Benet-Buchholz, J.; Poyatos, M.; Llobet, A. *J. Am. Chem. Soc.* **2006**, *128*, 5306.
(4) Lebeau, E. L.; Adeyemi, S. J.; Meyer, T. J. *Inorg. Chem.* **1998**, *37*, 6476.
(5) Meyer, T. J.; Huynh, M. H. V. *Inorg. Chem.* **2003**, *42*, 8140.
(6) (a) Meyer, G. J. *Inorg. Chem.* **2005**, *44*, 6852. (b) Grätzel, M. *Inorg. Chem.* **2005**, *44*, 6841.
(7) Monnereau, C.; Gomez, J.; Blart, E.; Odobel, F.; Wallin, S.; Fallberg, A.; Hammarström, L. *Inorg. Chem.* **2005**, *44*, 4806.
(8) Bard, A. J.; Faulkner, L. R. *Electrochemical Methods: Fundamentals and Applications*, 2nd ed.; John Wiley: New York, 2001.
(9) Hornstein, B. J.; Dattelbaum, D. M.; Schoonover, J. R.; Meyer, T. J. *Inorg. Chem.* Submitted.

JA068630+